Second-order motion-compensated spin echo diffusion tensor imaging of the human heart

Christian T. Stoeck, Constantin von Deuster, Martin Genet, David Atkinson, Sebastian Kozerke

Higher Order Motion Compensated Spin-Echo Diffusion Tensor Imaging of the Human Heart

Christian T. Stoeck[1], Constantin von Deuster[1,2], Martin Genet[1], David Atkinson[3], Sebastian Kozerke[1,2]

[1]Institute for Biomedical Engineering, University and ETH Zurich, Zurich, Switzerland
[2]Imaging Sciences and Biomedical Engineering, King's College London, London, United Kingdom
[3]Centre for Medical Imaging, University College London, London, United Kingdom

Running title: Cardiac DTI Using Spin-Echoes

Submission: Technical Note

Word Count: (2632)

Mailing Address: Sebastian Kozerke, PhD
Institute for Biomedical Engineering
University and ETH Zurich
Gloriastrasse 35
8092 Zurich
Tel.: + 41 44 632 3549
FAX: + 41 44 632 1193
Email: kozerke@biomed.ee.ethz.ch

Abstract

Purpose

Myocardial microstructure has been challenging to probe in-vivo. Diffusion weighted spin echo sequences as alternative to diffusion weighted stimulated echo imaging for cardiac diffusion tensor imaging (DTI) are highly sensitive to cardiac bulk motion. In this work the use of second order motion compensated diffusion encoding is compared to previously presented first order motion compensation for DTI during systolic contraction.

Methods

First and second order motion compensated diffusion encoding gradients were incorporated into a single-shot spin-echo sequence. The effect of myocardial strain on the apparent diffusion coefficients as a function of trigger delay was investigated in-vivo. Spin-echo based cardiac diffusion weighted imaging (DWI) and DTI was acquired at various trigger delays during systolic contraction at basal and apical level.

Results

For first order motion compensated diffusion encoding a timing window of about 40% of systolic contraction in duration was found around 60% peak systole for in-vivo DTI. With second order motion compensating gradients only very early trigger delays below 37.5% peak systole at the apical level appeared defective. At basal level DTI was successfully acquired over the entire range of trigger delays from 37.5%-75% peak systole.

Conclusion

Second order motion compensated gradients are less sensitive to sequence timing and allow for diffusion weighting at the apex and the base with the same trigger delay without optimization of the sequence trigger delay.

Key words: in-vivo cardiac DTI, diffusion tensor imaging, spin-echo, myocardial microstructure

Introduction

Ex-vivo diffusion tensor imaging (DTI) and diffusion spectrum imaging (DSI) have provided invaluable insights into myocardial fibre architecture of the human heart (1-3). While a static view of cardiac myofiber arrangement is of interest, it cannot address some of the crucial questions related to dynamic rearrangement of myofiber aggregates during the cardiac cycle. Moreover, the study of longitudinal microscopic changes of myocardium in a range of relevant cardiovascular diseases necessitates in-vivo imaging of the human heart.

Up to date only a limited number of studies have demonstrated the feasibility of diffusion weighted imaging of the *in-vivo* human heart (4-13). The lack of data is due to the fact that *in-vivo* cardiac DTI faces considerable challenges in relation to bulk motion and myocardial strain during diffusion encoding.

Two sequence types have been investigated for *in-vivo* DTI. The STimulated Echo Acquisition Mode (STEAM) was initially proposed for cardiac diffusion weighted imaging (DWI) (14) and subsequently used to perform DTI during breath holds (5,6,15) and during free breathing in combination with patient feedback control (16). The advantage of STEAM based sequences is its feasibility on standard clinical MR systems, without the need for high-performance gradient hardware. The nature of STEAM imaging, however, requires echo encoding across two consecutive heart beats while the heart needs to be spatially aligned within narrow limits. As a consequence of this fact and the required motion control, exam times are very long and considerable patient cooperation is required. In addition, there is an intrinsic weighting of the diffusion signal due to myocardial strain (4,17). This issue may be addressed by imaging in the so-called “sweet spots” (5) which, however, limit imaging to two predefined cardiac phases which do not coincide with end systole and end diastole. Alternatively, strain correction may be applied in post-processing based on the knowledge of the time course of myocardial strain (17) .

Diffusion weighted single-shot spin-echo (SE) imaging has been proposed as an alternative to STEAM and has been demonstrated to provide diffusion tensor information of the in-vivo human heart (7-10,12,18,19). The acquisition scheme permits free-breathing imaging without the need for dedicated patient feedback. However, direct strain encoding due to bulk motion during the application of the diffusion gradients needs to be addressed. To minimize strain effects, spin-echo DWI and DTI have primarily been applied in diastole (12,13,20).

An approach to overcome signal attenuation caused by changes in cardiac strain is to design higher-order motion compensated diffusion gradient waveforms, which can be used as part of SE schemes (20) or as part of T_2 pre-pulses (21). The latter variant, however, may be very sensitive to residual phase due to RF pulse imperfections and uncompensated cardiac motion components.

Finally, image post-processing methods may be employed to correct for strain-induced signal attenuation of conventional twice-refocused diffusion weighted SE images. To this end, diffusion weighted images are acquired at different trigger delays during the diastolic rest period (12,13) and temporal filtering and projection is used to combined image information from the set of temporally resolved images (22). Potential drawbacks of the approach, however, include the fact that the myocardium is thinnest in diastole and hence partial voluming is enhanced. In addition, diffusion weighting is limited to rather low b-values which reduces diffusion related contrast and perfusion induced signal attenuation may confound results.

Systolic cardiac DTI in humans has been proposed based on first order motion compensated diffusion gradients incorporated into a SE sequence (7,8,23). With this approach, careful sequence timing is required when applied on clinical MR imaging equipment (19). Stronger gradient systems on animal imaging systems delivering up to 1.5T/m maximum gradient amplitudes allow for significantly reduced diffusion gradient durations (11) and third order gradient moment nulling was investigated in the in-vivo rat heart (24).

The objective of the present work is to propose and implement second order motion compensated spin-echo diffusion tensor imaging of the human heart on a clinical scanner. The effect of strain on images of fibre architecture of the in-vivo left ventricle is investigated and compared for first and second order motion compensated imaging.

Methods

The signal phase accumulated during diffusion encoding is described by $\varphi(\vec{r}(t)) = \gamma \int_0^{t_{encoding}} \vec{G}(t)\vec{r}(t)dt$ with $t_{encoding}$ representing the duration of the diffusion gradient, $\vec{G}(t)$ the gradient waveform and $\vec{r}(t)$ the spatial trajectory of the spin. Upon Taylor expansion of $\vec{r}(t)$ the phase can be written as:

$$\varphi_{t_{encoding}} = \gamma \int_0^{t_{encoding}} \vec{G}(t)\vec{x}_{t=0}dt + \gamma \int_0^{t_{encoding}} \vec{G}(t)\dot{\vec{x}}_{t=0}tdt + \frac{\gamma}{2}\int_0^{t_{encoding}} G(t)\ddot{\vec{x}}_{t=0}t^2dt + ... \quad [1]$$

with the associated n[th] order gradient moments $\vec{m}_n$:

$$\vec{m}_0 = \int_0^{t_{encoding}} \vec{G}(t)dt$$
$$\vec{m}_1 = \int_0^{t_{encoding}} t\vec{G}(t)dt$$
$$\vec{m}_2 = \int_0^{t_{encoding}} t^2\vec{G}(t)dt$$
$$\vdots$$
$$\vec{m}_n = \int_0^{t_{encoding}} t^n\vec{G}(t)dt$$

From equation [1] it is evident that nulling of higher order moments results in phase insensitivity to higher order motion. To minimize the total diffusion gradient duration for a given b-value, and hence echo time, higher order moment nulling was implemented by modifying gradient duration while utilizing the maximum gradient amplitude. Figure **1** a) illustrates a first order motion compensated (MC) gradient waveform (7,11) with $m_0 = m_1 = 0$ at $t = t_{encoding}$. Both, first and second order motion compensation is achieved with the gradient waveform presented in Figure 1 b) with $m_0 = m_1 = m_2 = 0$ at $t = t_{encoding}$.

Study protocol

First and second order motion compensated diffusion tensor imaging were implemented on a clinical 1.5T Philips Achieva System (Philips Healthcare, Best, The Netherlands) equipped with a gradient system delivering 80mT/m per physical axis at a slew rate of 100mT/m/ms.

Five subjects (4 female, age: 21±2years, heart rate: 66±13 beats/min, min/max heart rate: 47/85 beats/min) with no known cardiac disease were imaged. Written informed consent was obtained from all subjects prior to scanning and the protocol was approved by the institutional review and ethics boards.

Diffusion imaging was performed in short-axis view orientation. A reduced field-of-view (FOV) technique was applied (25) employing a spectral spatial pulse for fat suppression (26). The duration of the 180° refocusing pulse was minimized using variable rate selective excitation (VERSE) (27) (Figure **1**). Imaging parameters were as follows: in plane resolution: 2.2×2.2mm^2, slice thickness: 6mm, field of view (FOV): 230×98mm^2, TR/TE: 1R-R/83ms, flip angle: heart rate dependent Ernst angle assuming a T_1 of 1030ms (28). The echo time was kept equal for both diffusion encoding approaches. The only parameter changed was the waveform of the diffusion encoding gradients.

Images were acquired during free breathing and gated by using a respiratory navigator with an acceptance window of 5mm. To suppress blood signal from orthogonal excitation, magnetization was saturated in a slab parallel to the imaging slice located apically.

Diffusion weighted imaging was performed at intervals of 10ms covering shortest trigger delay possible (45ms) to peak systole (time point of maximal circumferential contraction). At each trigger delay eight signal averages of a b=0 image as well as three diffusion encoded images with encoding direction in readout, phase-encoding and through-slice direction with a b-value of 450s/mm^2 were acquired. Slices were positioned at basal and apical locations (Figure **2**), at which rotational motion and through-plane contraction are largest.

In one volunteer, DTI data with ten diffusion encoding directions (29) were acquired additionally. The sequence parameters were identical to prior DWI, except for using a TR of 2R-R intervals

and 10 signal averages. Data was acquired at basal and apical level at 38%, 47%, 56%, 66% and 75% peak systole employing both first and second order motion compensated gradient schemes.

Data analysis

The apparent diffusion coefficient (ADC) was calculated for each data set for the different trigger delay and diffusion directions acquired. The mean ADC and the corresponding standard deviation within each slice were analysed across the myocardium (30). The trigger delay is reported as percentage values relative to peak systole (100% peak systole). Upon estimation of the diffusion tensors, mean diffusivity (MD), fractional anisotropy (FA) were calculated. To avoid partial volume effects of bright blood signal in the b0 image, the mean diffusion image was scaled and used as b0 reference for myofiber angle analysis. From the diffusion tensors, the local helix, transverse and sheet angles were calculated as in previous work (8,23,31). The transmural course of the helix angle and the angle histograms of the sheet angle were estimated in each slice for the entire myocardium. Helix and sheet angle maps were calculated for each heart phase. The transverse angle is reported as mean± standard deviation across the myocardium. The resulting diffusion tensors are visualized by superquadric glyphs. To visualize strain induced errors, the tensor were color-coded according to the local transverse angle.

Results

In Figure **2** ADC values measured based on encoding along readout (M), phase encode (P) and slice select (S) directions as well as MD values as function of the trigger delay are shown. Second order motion compensated diffusion encoding yields MD values within its minimum and 10% above the minimum at a trigger delay of 21% to 77% for the apical and 20% to 64% peak systole for the basal slices. In comparison, applying first order motion compensation only, the corresponding trigger delays windows are only 45% to 55% and 29% to 51% end systole for the apical and basal slice, respectively.

The standard deviation of ADCs and MDs across the myocardium was found to be consistently lower for second order relative to first order motion compensated diffusion encoding. MD values for a trigger delay of 75% peak systole are reported for first and second order motion compensation in Table 1. It is noted that MD values are overestimated by up to 60% and 80% with first order relative to second order motion compensation for apical and basal slices, respectively.

Figure **3** shows diffusion tensors at apical and basal level for 38%, 47%, 56%, 66% and 75% peak systole (cmp. volunteer #4 in Table 1). Glyphs are color-coded according to the local transverse myofiber angle. For first order motion compensated diffusion encoding, patches of high transverse angulation (±90°) are visible. Second order motion compensation results in better circumferential alignment of the principal diffusion direction. Using second order motion compensated gradients, the standard deviation of the transverse angle at basal level is in the range of 20° for all trigger delays. At the apex, imaging at trigger delays from 47%-75% results in the same angle variation. For first order motion compensated diffusion encoding similar angle variation are found only for 56% peak systole at basal level.

Figure **4** shows the helix angle maps corresponding to the slices presented in Figure **3**. For second order motion compensated diffusion encoding a linear helix angle course as function of

the transmural depth is seen. At apical level similar helix angle distributions are found comparing both diffusion encoding methods, with a larger variation across sectors for first order motion compensation. Patches of high angulation (dark blue/red) are found throughout the myocardium. At basal level and trigger delays other than 65% peak systole, areas of single helix direction without any transmural course are present with first order motion compensation. The expected transmural course of helix angles across the segments is again absent for the late trigger delay of 75% peak systole.

Figure **5** shows sheet angle maps corresponding to the slices presented in Figure **3**. For first order motion compensated encoding no coherent angle distribution as a function of trigger delays is found, while similar patterns are present for 47%-75% systole when second order motion compensation is used. Similar sheet angle maps obtained from both encoding schemes are found at basal level for a trigger delay of 56% peak systole. The angle histograms show a shift from highly angulated myolaminae towards lower angulation over the course of trigger delays.

Discussion

In the present study, second order motion compensated cardiac diffusion Imaging has been implemented on a clinical MR system and compared to first order motion compensation.

While MD values across the myocardium were found to be relatively constant over a wide range of trigger delays for second order motion compensated diffusion encoding, first order motion compensated diffusion encoding has resulted in a strong dependency on the trigger delay in accordance to previous findings (32). Second order motion compensated diffusion encoding not only yielded reduced variation of MD values within the myocardium, it also reduced standard deviation of MD values across volunteers.

For first order motion compensated diffusion encoding the optimal trigger delay was found between 50% and 60% peak systole (7,19). Tensor reconstruction confirmed that the window of feasible trigger delays is narrow. At ±30ms offset from the optimal trigger delay time, tensors alignment deviated locally from the expected circumferential arrangement. At the apex, even with the optimal trigger delay a patch of large helix angles was found in the posterior segment, indicating strain induced artefacts. Patches of high helix angulations in the apex were found to correspond to areas exhibiting large transverse angles.

In this study the helix angle was calculated upon projection of the first eigenvector onto a cylindrical surface (31). Hence large deviations from a circumferential course result in an overestimation of the helix angle. At basal level, considerable through-plane motion occurs leading to loss of the characteristic helix angle distribution for the first half of systole.

For second order motion compensated diffusion encoding a wider window of trigger delays was found. A coherent circumferential course of myofibers with a linear transmural helix distribution was detected. The results are in line with previously reported fibre angulations in the ex-vivo human heart (33).

The pattern of sheet angles found with second order motion compensated encoding were in line with data reported in excised animal hearts (34).

In this study, the echo time was kept the same for both diffusion encoding gradient waveforms to ensure similar T_2 weighting. For first order motion compensated encoding the echo time may, however, be reduced by 4ms.

With second order motion compensated diffusion encoding in-vivo cardiac DTI at the apex was feasible. Besides the large degree of rotational motion present, imaging the apex is subject to partial volume effects. The apical myocardium is thinner compared to the base and its curvature is stronger. Additionally blood remains more static at the apex leading to insufficient blood suppression and leakage of bright blood signal into voxels at the border of the myocardium. To reduce partial volume effects higher spatial resolution is desired. By use of parallel imaging

techniques spatial resolution could be increased without prolonging echo time at the cost of reduced SNR (35,36).

For the second order motion compensated gradient waveform used in this study the gap between both gradient lobes depends on the desired b-value. To ensure sufficient time for the echo pulse, a minimum b-value is necessary. Achieving lower b-values can hence not be realized by shortening gradient duration, but requires reducing the maximum gradient strength. However, unlike the first order motion compensated encoding scheme, the gradient's zeroth moment at the position of the echo pulse is different from zero for the second order motion compensated scheme. Hence FID crushing gradients on either side of the echo pulse may be removed.

In this study a clinically available high performance gradient system was employed enabling gradient duration of 43ms/50ms for first/second order motion compensated gradient schemes. For clinical systems with lower maximum gradient strengths such as 60mT/m or 40mT/m the total gradient duration increases to 51ms/60ms and 64ms/78ms. Prolonged gradient duration increases the sensitivity to motion, since bulk motion is more likely to deviate from its first and second order Taylor approximation.

Conclusion

In this study second order motion compensated spin-echo diffusion encoding was implemented and compared relative to first order motion compensated diffusion gradient waveforms for systolic cardiac diffusion tensor imaging. A significantly decreased sensitivity to bulk motion was found compared to first order motion compensated diffusion gradients, enabling cardiac DTI at various time points during systolic contraction without the need for optimization of sequence trigger delays.

Acknowledgement

The authors acknowledge funding by the Swiss National Science Foundation, grant #CR3213_132671/1, UK EPSRC (EP/I018700/1), Adult Congenital Heart Disease Service GSTT and the National Institute for Health Research (NIHR) Biomedical Research Centre at Guy's and St Thomas' NHS Foundation Trust and King's College London. The views expressed are those of the authors and not necessarily those of the NHS, the NIHR or the Department of Health.

Bibliography

1. **Lombaert H, Peyrat J-M, Fanton L, Cheriet F, Delingette H, Ayache N, Clarysse P, Magnin I, Croisille P. Variability of the Human Cardiac Laminar Structure. 2012;7085:160-167.**
2. **Sosnovik DE, Wang R, Dai G, Reese TG, Wedeen VJ. Diffusion MR tractography of the heart. J Cardiovasc Magn Reson 2009;11:47.**
3. **Sosnovik DE, Wang R, Dai G, Wang T, Aikawa E, Novikov M, Rosenzweig A, Gilbert RJ, Wedeen VJ. Diffusion spectrum MRI tractography reveals the presence of a complex network of residual myofibers in infarcted myocardium. Circ Cardiovasc Imaging 2009;2(3):206-212.**
4. **Reese TG, Weisskoff RM, Smith RN, Rosen BR, Dinsmore RE, Wedeen VJ. Imaging myocardial fiber architecture in vivo with magnetic resonance. Magnetic Resonance in Medicine 1995;34(6):786-791.**
5. **Tseng WY, Reese TG, Weisskoff RM, Wedeen VJ. Cardiac diffusion tensor MRI in vivo without strain correction. Magn Reson Med 1999;42(2):393-403.**
6. **Dou J, Reese TG, Tseng WY, Wedeen VJ. Cardiac diffusion MRI without motion effects. Magn Reson Med 2002;48(1):105-114.**
7. **Gamper U, Boesiger P, Kozerke S. Diffusion imaging of the in vivo heart using spin echoes-considerations on bulk motion sensitivity. Magn Reson Med 2007;57(2):331-337.**
8. **Toussaint N, Sermesant M, Stoeck CT, Kozerke S, Batchelor PG. In vivo human 3D cardiac fibre architecture: reconstruction using curvilinear interpolation of diffusion tensor images. Med Image Comput Comput Assist Interv 2010;13(Pt 1):418-425.**
9. **Toussaint N, Stoeck CT, Schaeffter T, Kozerke S, Sermesant M, Batchelor PG. In vivo human cardiac fibre architecture estimation using shape-based diffusion tensor processing. Medical image analysis 2013;17(8):1243-1255.**
10. **Froeling M, Strijkers GJ, Nederveen AJ, Chamuleau SA, Luijten PR. Diffusion Tensor MRI of the Heart–In Vivo Imaging of Myocardial Fiber Architecture. Current Cardiovascular Imaging Reports 2014;7(7):1-11.**
11. **Sosnovik DE, Mekkaoui C, Huang S, Chen HH, Dai G, Stoeck CT, Ngoy S, Guan J, Wang R, Kostis WJ, Jackowski MP, Wedeen VJ, Kozerke S, Liao R. Microstructural impact of ischemia and bone marrow-derived cell therapy revealed with diffusion tensor magnetic resonance imaging tractography of the heart in vivo. Circulation 2014;129(17):1731-1741.**
12. **Wei H, Viallon M, Delattre BM, Wang L, Pai VM, Wen H, Xue H, Guetter C, Croisille P, Zhu Y. Assessment of cardiac motion effects on the fiber architecture of the human heart in vivo. IEEE transactions on medical imaging 2013;32(10):1928-1938.**
13. **Rapacchi S, Wen H, Viallon M, Grenier D, Kellman P, Croisille P, Pai VM. Low b-value diffusion-weighted cardiac magnetic resonance imaging: initial results in humans using an optimal time-window imaging approach. Invest Radiol 2011;46(12):751-758.**
14. **Edelman RR, Gaa J, Wedeen VJ, Loh E, Hare JM, Prasad P, Li W. In vivo measurement of water diffusion in the human heart. Magn Reson Med 1994;32(3):423-428.**

15. **Dou J, Tseng WY, Reese TG, Wedeen VJ. Combined diffusion and strain MRI reveals structure and function of human myocardial laminar sheets in vivo. Magn Reson Med 2003;50(1):107-113.**
16. **Nielles-Vallespin S, Mekkaoui C, Gatehouse P, Reese T, Keegan J, Collins S, Speier P, Feiweier T, Jackowski M, Sosnovik D, Firmin D. Diffusion tensor MRI of the human heart In Vivo with a navigator based free breathing approach. Journal of Cardiovascular Magnetic Resonance 2012;14(0):1-2.**
17. **Reese TG, Wedeen VJ, Weisskoff RM. Measuring diffusion in the presence of material strain. Journal of Magnetic Resonance, Series B 1996;112(3):253-258.**
18. **Stoeck CT, von Deuster C, Toussaint N, Kozerke S. High-resolution single-shot DTI of the in-vivo human heart using asymmetric diffusion encoding. In Proceedings of the 21st Annual Meeting of ISMRM. Salt Lake City, Utah, USA. 2013. p 0480.**
19. **Stoeck CT, Toussaint N, Boesiger P, Batchelor PG, Kozerke S. Sequence timing optimization in multi-slice diffusion tensor imaging of the beating heart In Proceedings of the 19th Annual Meeting of ISMRM. Montréal, Canada. 2011. p 282.**
20. **Nakamura T, Shibukawa S, Muro I, Kajihara N, Nishio H, Ogini T, Niwa T, Imai Y. Improvement of visualization of cardiac wall in diffusion-weighted imaging using cardiac triggering and acceleration motion correction. In Proceedings of the 22nd Annual Meeting of ISMRM. Milan, Italy. 2014. p 2417.**
21. **Nguyen C, Fan Z, Sharif B, He Y, Dharmakumar R, Berman DS, Li D. In vivo three-dimensional high resolution cardiac diffusion-weighted MRI: A motion compensated diffusion-prepared balanced steady-state free precession approach. Magn Reson Med 2013.**
22. **Pai VM, Rapacchi S, Kellman P, Croisille P, Wen H. PCATMIP: enhancing signal intensity in diffusion-weighted magnetic resonance imaging. Magn Reson Med 2011;65(6):1611-1619.**
23. **Toussaint N, Souplet J-C, Fillard P. MedINRIA: Medical image navigation and research tool by INRIA. In Proceedings of the Proc of MICCAI. 2007.**
24. **Welsh CL, Dibella EV, Hsu EW. Analysis and Design of Higher-Order Motion-Compensated Diffusion Encoding Schemes for In Vivo Cardiac DTI. In Proceedings of the 22nd Annual Meeting of ISMRM. Milan, Italy. 2014. p 2436.**
25. **Feinberg DA, Hoenninger JC, Crooks LE, Kaufman L, Watts JC, Arakawa M. Inner volume MR imaging: technical concepts and their application. Radiology 1985;156(3):743-747.**
26. **Meyer CH, Pauly JM, Macovski A, Nishimura DG. Simultaneous spatial and spectral selective excitation. Magn Reson Med 1990;15(2):287-304.**
27. **Hargreaves BA, Cunningham CH, Nishimura DG, Conolly SM. Variable-rate selective excitation for rapid MRI sequences. Magn Reson Med 2004;52(3):590-597.**
28. **Stanisz GJ, Odrobina EE, Pun J, Escaravage M, Graham SJ, Bronskill MJ, Henkelman RM. T1, T2 relaxation and magnetization transfer in tissue at 3T. Magn Reson Med 2005;54(3):507-512.**
29. **Jones DK, Horsfield MA, Simmons A. Optimal strategies for measuring diffusion in anisotropic systems by magnetic resonance imaging. Magn Reson Med 1999;42(3):515-525.**
30. **Cerqueira MD, Weissman NJ, Dilsizian V, Jacobs AK, Kaul S, Laskey WK, Pennell DJ, Rumberger JA, Ryan T, Verani MS. Standardized myocardial segmentation and nomenclature for tomographic imaging of the heart: a statement for healthcare professionals from the Cardiac Imaging Committee of the Council on Clinical Cardiology of the American Heart Association. Circulation 2002;105(4):539-542.**

31. **Scollan DF, Holmes A, Winslow R, Forder J. Histological validation of myocardial microstructure obtained from diffusion tensor magnetic resonance imaging. The American journal of physiology 1998;275(6 Pt 2):H2308-2318.**
32. **Stoeck CT, Hu P, Peters DC, Kissinger KV, Goddu B, Goepfert L, Ngo L, Manning WJ, Kozerke S, Nezafat R. Optimization of on-resonant magnetization transfer contrast in coronary vein MRI. Magn Reson Med 2010;64(6):1849-1854.**
33. **Lombaert H, Peyrat J-M, Croisille P, Rapacchi S, Fanton L, Clarysse P, Delingette H, Ayache N. Statistical analysis of the human cardiac fiber architecture from DT-MRI. Functional Imaging and Modeling of the Heart: Springer; 2011. p 171-179.**
34. **Hales PW, Schneider JE, Burton RA, Wright BJ, Bollensdorff C, Kohl P. Histo-anatomical structure of the living isolated rat heart in two contraction states assessed by diffusion tensor MRI. Progress in biophysics and molecular biology 2012;110(2-3):319-330.**
35. **Pruessmann KP, Weiger M, Scheidegger MB, Boesiger P. SENSE: sensitivity encoding for fast MRI. Magn Reson Med 1999;42(5):952-962.**
36. **Griswold MA, Jakob PM, Heidemann RM, Nittka M, Jellus V, Wang J, Kiefer B, Haase A. Generalized autocalibrating partially parallel acquisitions (GRAPPA). Magn Reson Med 2002;47(6):1202-1210.**

Table

$1^{st}/2^{nd}$ MC		mean	SD	$1^{st}/2^{nd}$ MC		mean	SD
MD apex [$10^{-4}mm^2/s$]	vol 1	12.1/12.6	2.9/2.3	MD base [$10^{-4}mm^2/s$]	vol 1	10.2/9.1	2.7/1.8
	vol 2	9.9/7.9	6.7/2.4		vol 2	9.7/7.2	2.7/2.2
	vol 3	18.3/11.3	4.1/1.7		vol 3	20.1/11.0	2.5/2.1
	vol 4	16.4/12.4	3.0/2.1		vol 4	14.8/10.0	1.8/1.8
	vol 5	10.4/10.7	2.8/2.2		vol 5	10.3/9.4	3.2/2.4

Table 1 Comparison of MD values at apical and basal level in the five volunteers for first and second order motion compensated (MC) diffusion imaging at 75% end-systole. The MD values are reported as mean and standard deviation (SD) across the myocardium.

Figures

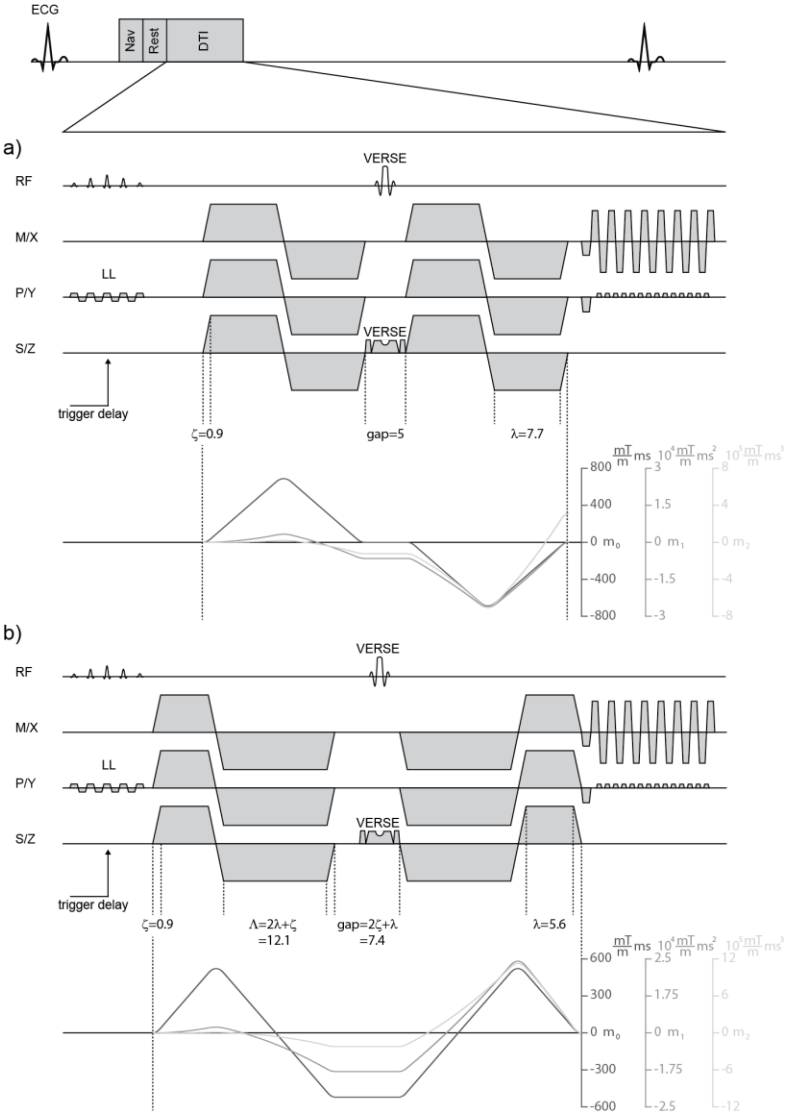

Figure 1 First (a) and second (b) order motion compensated diffusion encoding using spin-echoes. Following a respiratory navigator (Nav), regional saturation (REST) is applied parallel to the imaging slice to saturate blood signal apically of the imaging slice. A spatial spectral pulse for fat suppression is used for reduced field of view imaging (LL). A variable rate selective excitation (VERSE) pulse is integrated for RF refocussing. The timing of gradients is given in ms. For each gradient waveform the 0^{th} to 2^{nd} moments (m_0, m_1, m_2) are plotted as function of time.

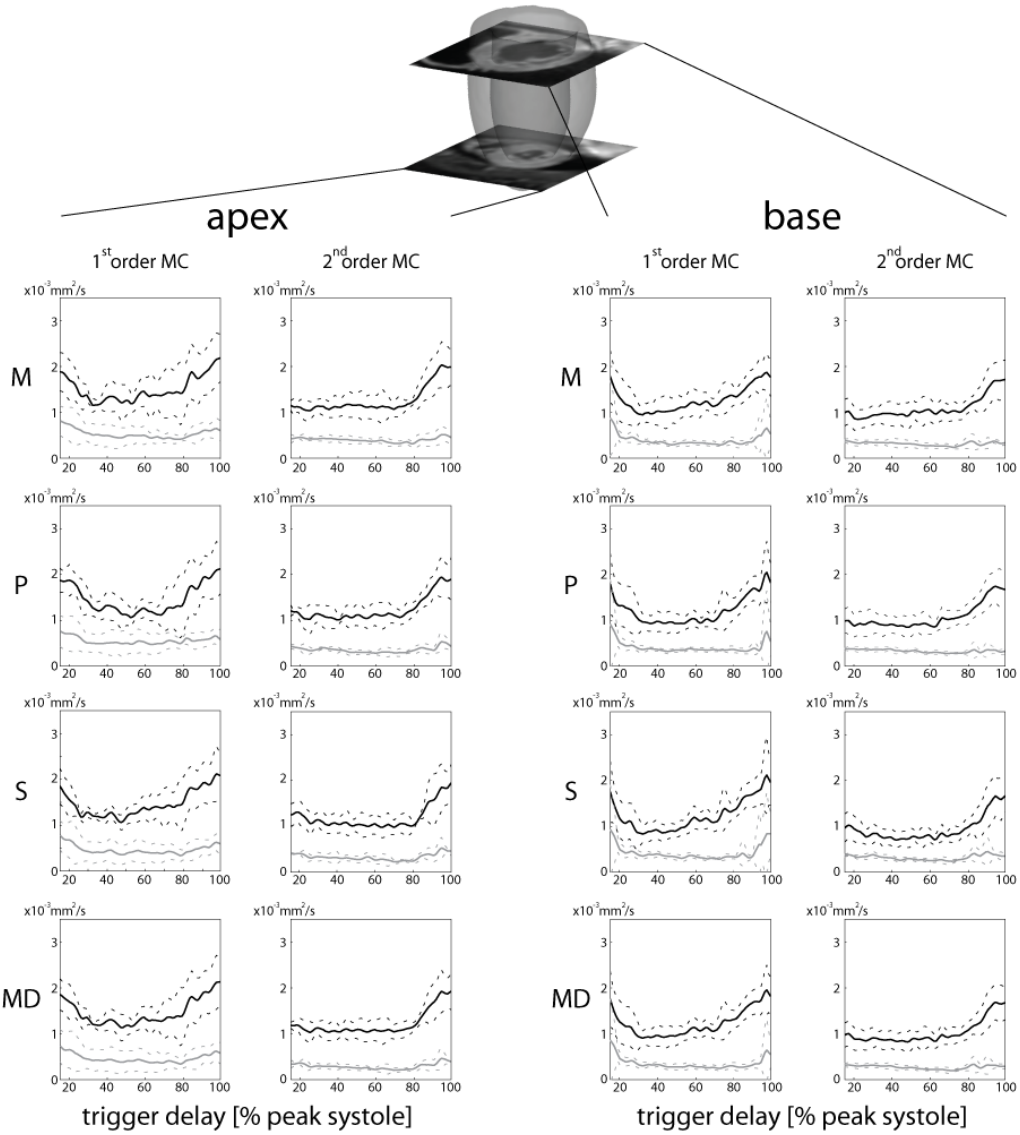

Figure 2 Apparent Diffusion Coefficients (ADC) for in-plane (M,P) and through-plane (S) encoding and Mean Diffusivity (MD) for first and second order motion compensated (MC) diffusion encoding as function of the trigger delay (in % peak systole) for an apical and basal slice location. Average values per slice are shown (in black) along with the standard deviation (in grey). Solid lines correspond to the mean across the volunteers and dashed lines to standard deviation.

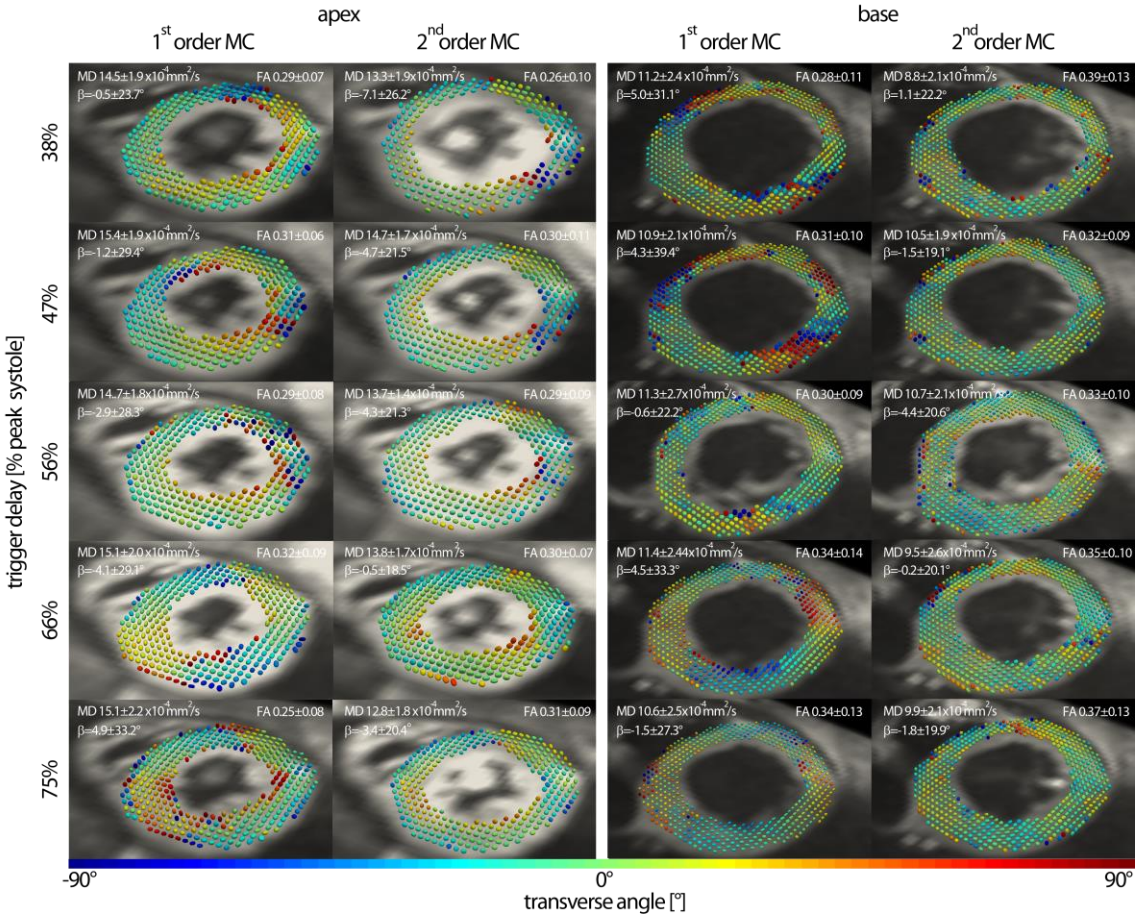

Figure 3 Superquadric glyph representation of the diffusion tensor at apical and basal level for different trigger delays. The colour coding corresponds to transverse angle β of the myocardial fibre.

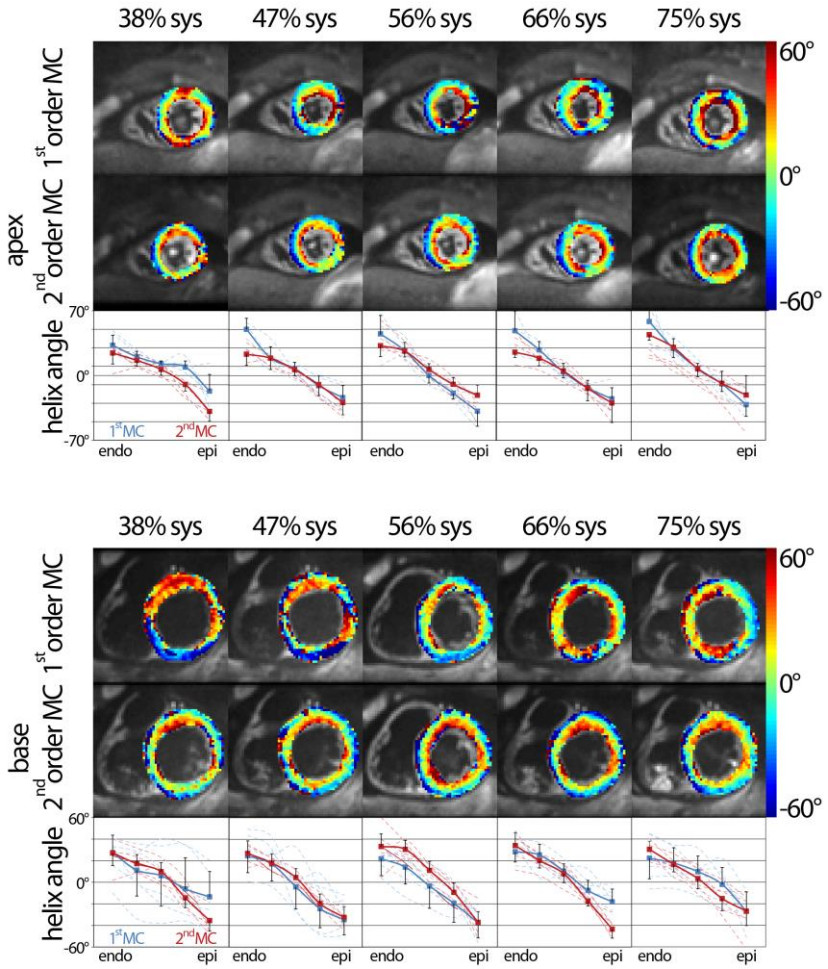

Figure 4. Helix analysis at apical (top) and basal (bottom) position. The transmural course of the helix angle is presented for first order motion compensated (blue) and second order motion compensated gradient waveforms. The solid lines correspond to the course of the helix angle considering the entire myocardium, and the dashed lines to the course for each AHA segment (4 segments apex, 6 segments base). The error bars corresponds to the standard deviation across the AHA segments within each slice.

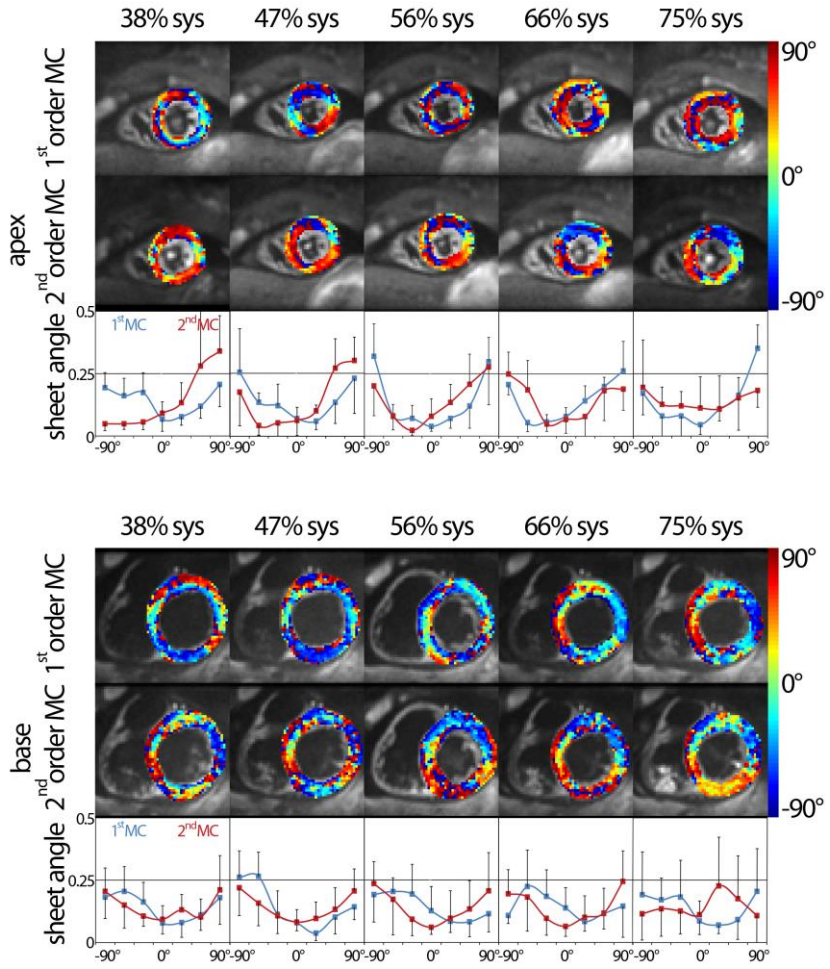

Figure 5 Sheet analysis at apical (top) and basal (bottom) position. The sheet angle histograms are presented for first order motion compensated (blue) and second order motion compensated gradient waveforms. The solid lines correspond to the counts of the sheet angles considering the entire myocardium, and the error bars to the standard deviation across AHA segments (4 segments apex, 6 segments base). Histograms are normalized.